energies

MDPI

Article

Research on the Starting Acceleration Characteristics of a New Mechanical–Electric–Hydraulic Power Coupling Electric Vehicle

Jian Yang [1,2], Tiezhu Zhang [1,2], Hongxin Zhang [1,2,*], Jichao Hong [3,*] and Zewen Meng [1,2]

1 College of Mechanical and Electrical Engineering, Qingdao University, Qingdao 260071, China; yangxiaoming8533@163.com (J.Y.); zhangtz@sdut.edu.cn (T.Z.); mengzewen@163.com (Z.M.)
2 Power Integration and Energy Storage Systems Engineering Technology Center (Qingdao), Qingdao 260071, China
3 School of Mechanical Engineering, University of Science and Technology Beijing, Beijing 100083, China
* Correspondence: zhx@qdu.edu.cn (H.Z.); hongjichao@ustb.edu.cn (J.H.)

Received: 30 October 2020; Accepted: 27 November 2020; Published: 28 November 2020

check for updates

Abstract: To simplify the layout of a purely electric vehicle transmission system and improve the acceleration performance of the vehicle, this paper utilizes the characteristics of the large torque of a hydraulic transmission system and proposes a new mechanical–electric–hydraulic dynamic coupling drive system (MEH-DCDS). It integrates the traditional motor and the swashplate hydraulic pump/motor into one, which can realize the mutual conversion between the mechanical energy, electrical energy, and hydraulic energy. This article explains its working principle and structural characteristics. At the same time, the mathematical model for the key components is established and the operation mode is divided into various types. Based on AMESim software, the article studies the dynamic characteristics of the MEH-DCDS, and finally proposes a method that combines real-time feedback of the accumulator output torque with PID control to complete the system simulation. The results show that the MEH-DCDS vehicle has a starting time of 4.52 s at ignition, and the starting performance is improved by 40.37% compared to that of a pure motor drive system vehicle; after a PID adjustment, the MEH-DCDS vehicle's starting time is shortened by 1.04 s, and the acceleration performance is improved by 23.01%. The results indicated the feasibility of the system and the power performance was substantially improved. Finally, the system is integrated into the vehicle and the dynamic performance of the MEH-DCDS under cycle conditions is verified by joint simulation. The results show that the vehicle is able to follow the control speed well when the MEH-DCDS is loaded on the vehicle. The state-of-charge (SOC) consumption rate is reduced by 20.33% compared to an electric vehicle, while the MEH-DCDS has an increased range of 45.7 m compared to the EV. This improves the energy efficiency and increases the driving range.

Keywords: mechanical–electric–hydraulic; coupling; PID; AMESim; Simulink

1. Introduction

With the development of electronic technology, especially the continuous improvement of power battery technology, storage batteries are widely used in the field of hybrid transportation. Energy storage batteries have a very high energy density and a very large storage capacity [1]. It also has good temperature performance and high rate discharge performance [2]. They also have a longer service life [3]. However, for purely electric vehicles, low-speed and heavy-duty vehicles, passenger cars, trucks, etc., the instantaneous high torque demand at ignition causes a large discharge current impact on the battery [4], which consumes much of the power and reduces the cycle life of the battery [5], decreasing the driving range of the vehicle [6]. Guo et al. [7] found that battery energy storage realizes energy recovery and reuse through the traditional power hybrid path. Wang et al. [8] developed a model that considers carbon emissions to simulate the recycling of electric vehicle batteries. A real-life case study of an electric vehicle manufacturer in China achieved a 5.7% reduction in total cost and a 21.8% reduction in CO_2 emissions. At this stage, the technology is relatively mature and has been widely used in urban buses, but its shortcomings include charging and discharging, a low frequency, low power density, and high price.

Zhao et al. [9] presented a novel hydraulic/electric synergistic power system with multiple modes of operation. In this paper, the component sizes of a hybrid electric vehicle (HEV), hydraulic hybrid vehicle (HHV) and hydraulic/electric synergistic vehicle (HESV) are selected based on the dynamic performance of the target vehicle. Fiala et al. [10] introduced the principle of a hydraulic accumulator and applied the hydraulic accumulator in purely electric vehicles as a power source for auxiliary drive. Sun et al. [11] proposed an energy-saving solution for a parallel hydraulic hybrid power system. This gives full play to the advantages of the hydraulic accumulator's high power density and its ability to efficiently store and release large amounts of energy, which can effectively overcome the disadvantages of battery energy storage. At the same time, it is relatively inexpensive and has a broader application prospect. Pugi et al. [12] presented an on-board hydraulic drive system capable of efficient recovery of braking energy. The system was subsequently applied in practice with a truck equipped with a hydraulic tool for waste collection. The design, assembly and testing of the system prototype showed that the efficiency of the system was improved accordingly and that the proposed method was feasible. Wang et al. [13] combined the high energy density of hydraulic accumulators and designed a strategy to improve fuel economy. The results show that the average fuel consumption per gallon of the proposed strategy, compared with the rule-based control strategy and the proportional integral derivative controller-based control strategy, increased by 7.3% and 5.9%, respectively.

Pretto et al. [14] presented a simple and inexpensive electrification device for the problem of low profitability of light duty tricycles. The solution discusses the profitability of light truck electrification in terms of energy prices in different countries, which allows to upgrade existing vehicles with limited investment. Special attention is paid to the optimization of regenerative braking and its blending with mechanical braking to maximize autonomy and maintain vehicle stability. Very little research has been done on this new electro-hydraulic hybrid powertrain. The economics of the vehicle are one of the most pressing issues to be addressed before it can be truly marketed and industrialized.

Zhou et al. [15] proposed a set of parallel hydraulic hybrid vehicles that integrate conventional engines and hydraulic pump/motors to independently or jointly drive vehicles. The results show that the comfort and driving performance of the transition from the hydraulic mode to engine mode are improved. Niu et al. [16] proposed and designed a parallel electro-hydraulic hybrid power system and applied it to urban vehicles. The experimental results show that the system can reduce the discharge intensity of urban trucks by 30% and extend the mileage of urban buses by 50% under frequent urban operating conditions. Hwang et al. [17] designed a hydraulic hybrid vehicle and used reverse simulation to simulate the changes in torque and battery state-of-charge (SOC) during the cycle of the United States Environmental Protection Agency (EPA NYCC) in New York City. The simulation results show that the electric economy of the designed hydraulic hybrid vehicle is 36.51% higher than that of a purely electric vehicle. Sprengel et al. [18] proposed a new type of hybrid hydraulic structure and performed six operating modes on the test bench under urban cycle conditions, and the results showed that the fuel economy of the system is improved by 17.35%, while the energy consumption is reduced by 12.04% for this hybrid hydraulic hybrid compared with the series hydraulic hybrid power system. In 2017, Geng et al. [19] developed an electro-hydraulic hybrid power transmission system for urban vehicles. The simulation results showed that the battery discharge pressure of urban delivery trucks can be reduced by an average of 30%. In the best case, the mileage of urban buses can be extended by 50%. Midgley et al. [20] designed a hydraulic regenerative braking system composed of high- and low-pressure accumulators. The potential of the system for crossing a hilly terrain has been studied, and it was found that the system can reduce fuel consumption by 12.6% on V-shaped valley, and by 5.3% on real elevation profiles. Wang et al. [21] comprehensively used the advantages of the high energy density of the battery and hydraulic accumulator and established the AMESim and Simulink co-simulation model of the power transmission system, which verified the feasibility of the system. Finally, an experimental platform was built, and the effectiveness of the transmission system was verified through experiments.

In this paper, a hydraulic-assisted, mechanical–electric–hydraulic dynamic coupling drive system (MEH-DCDS) is designed that makes full use of the high power density of hydraulic power. It can integrate the traditional permanent magnet rotating motor with the swashplate axial plunger pump/motor, and it can mutually convert electrical energy, mechanical energy, and hydraulic energy. It can be widely used in automobiles, construction machinery, agricultural machinery, and machine tools. It is especially suitable as a power transmission device for electric commercial vehicles. The MEH-DCDS for the power system and the hydraulic system of the dynamic coupling was designed and integrated into an organic whole. It fully combines the advantages of the two, changes the driving method, and optimizes the structure of the transmission system. It greatly prolongs the service life of the battery and increases the mileage of the vehicle. At the same time, it significantly improves the power performance and fuel economy of vehicles.

2. The Working Principle of the MEH-DCDS

The MEH-DCDS is designed in combination with the working principle and characteristics of electro-hydraulic transmission [22–24]. Based on purely electric vehicles, high and low hydraulic accumulators are added. The electro-hydraulic coupler replaces the electric motor and the hydraulic pump/motor and can be torque-coupled to the output driving force, integrating mechanical energy, electrical energy, and hydraulic energy. It satisfies the application needs of many occasions and achieves better energy-saving effects through complementary advantages. During braking, part of the braking energy is recovered and stored in the hydraulic accumulator and battery for use in high-power demand conditions, such as starting and acceleration, which improves the starting characteristics of the vehicle, reduces the effect of high torque demand on the battery SOC and achieves the purpose of extending the service life of the battery and increases the driving range of the vehicle.

As shown in Figure 1, the MEH-DCDS vehicle includes an electro-hydraulic coupler, high-pressure accumulator (HPA), low-pressure accumulator (LPA), final drive/differential, clutch, secondary components, a power converter, vehicle controller, power battery pack, etc. The battery is the power source of the power system, and the electric power is the main power form of the power system. The hydraulic power is converted from electric power and plays an auxiliary driving role. When the system is working, the controller receives the acceleration signal, the brake signal, and the signal from the pressure sensor, and transmits it to the hydraulic control unit after the vehicle controller to adjust the displacement of the hydraulic pump/motor. When the vehicle starts, the electric power does not output power, the hydraulic pump/motor is used as the motor, and the hydraulic oil flows from the HPA to the LPA. After the hydraulic power drives the vehicle to accelerate to a certain lower speed, the motor traction system is involved in work to reduce the effect of a high current and high torque when the vehicle starts. If the pressure in the hydraulic accumulator reaches the minimum working pressure of the accumulator, the hydraulic power stops working, the motor selects the opportunity to drive the hydraulic pump/motor to charge the hydraulic accumulator in the blank working condition, and the hydraulic pump/motor is used as a pump. The oil flows from the LPA to the HPA. During the acceleration and climbing stage, electric power intervenes to work together with the hydraulic pump/motor to perform torque coupling and output power to drive the vehicle to accelerate and climb. During the constant-speed driving phase of the vehicle, because of the stable speed and small external load, the hydraulic system does not intervene in the work and only the electric power drives the vehicle to cruise. In idling conditions, electric power is used as a power source to drive the secondary components to work in the state of a hydraulic pump, pumping the oil of the LPA into the HPA, and at this time, the electrical energy is converted into hydraulic energy to store energy in the accumulator over time. When the vehicle is operating at a low speed, the hydraulic system recovers braking energy, and ABS braking is used for emergency braking without braking energy recovery. In other braking conditions, the braking energy is primarily recovered in the form of electrical energy at high speeds. At a medium speed, the braking energy is primarily recovered by electric and hydraulic energy at the same time.

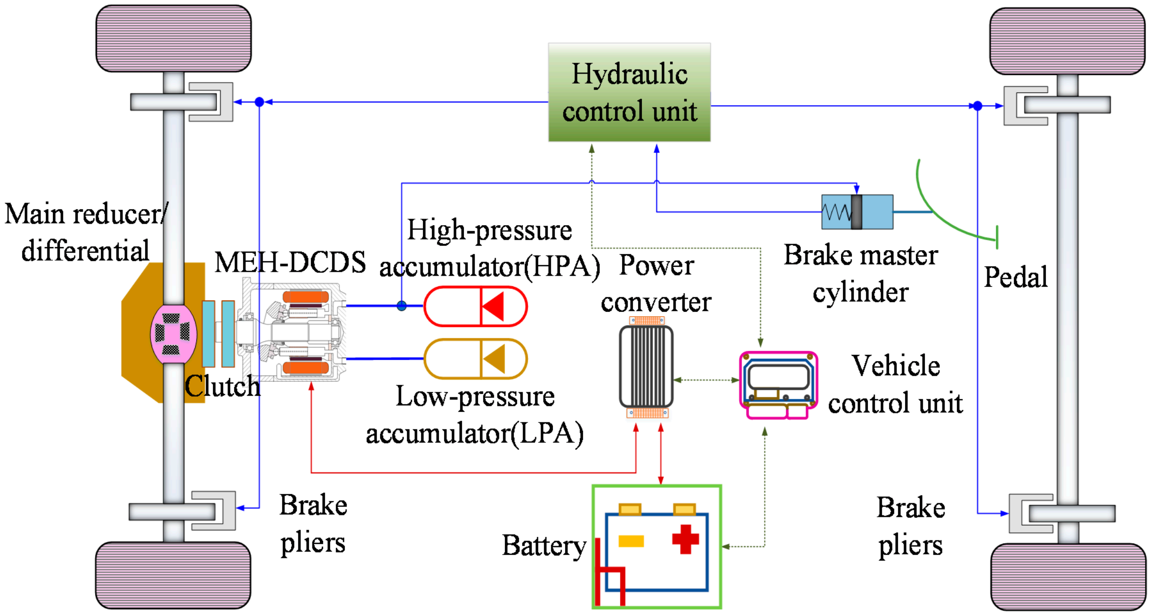

Figure 1. Structure of the mechanical–electric–hydraulic dynamic coupling drive system (MEH-DCDS).

Compared with traditional fuel vehicles and purely electric vehicles, the main advantages of the new MEH-DCDS are as follows:

(1) The MEH-DCDS replaces the drive motor, transmission, and auxiliary drive system of traditional electric commercial vehicles. It optimizes the structure of the transmission system. Various power conversions are optimally matched through structural parameters within the system, which improves the transmission efficiency and makes the entire power transmission system more efficient. It also has a self-cooling function and compact structure.
(2) Because of the high power density, hydraulic power can quickly start the car and double the car's grade ability. It substantially improves the dynamics of the vehicle and greatly reduces the peak power of the electric power; when the MEH-DCDS brakes, hydraulic regenerative braking, electric regenerative braking, and friction braking (ABS braking) work together. This design decreases the braking distance and results in a more stable recovery of hydraulic power (over 70%).
(3) The MEH-DCDS reduces the current impact caused by changes in vehicle load and the damage to the battery and electronic control system caused by the current impact. It reduces the utilization rate of the friction brake system, greatly improves the service life and reliability, and substantially increases the driving range.

3. Mathematical Modeling of the MEH-DCDS

The MEH-DCDS integrates electric power and hydraulic power [25], combining the traditional permanent magnet synchronous motor and hydraulic pump/motor into a whole, so the analysis of electric power includes battery and motor modules, and the analysis of hydraulic power is performed on the hydraulic pump/motor [26]. This part of the paper mainly establishes the mathematical models of hydraulic power, hydraulic accumulators, and electric power modules [27].

3.1. Hydraulic Power

When the vehicle starts, the secondary element is used as a hydraulic motor to drive the vehicle alone; when the vehicle is accelerating, the secondary element is used as a hydraulic motor, and the electric power is torque-coupled to output power; during braking, the secondary element is used as a hydraulic pump to store the excess braking energy in the hydraulic accumulator in the form of hydraulic energy [28,29].

The swashplate opening β and output torque T_p of the hydraulic pump/motor can be described as

$$\begin{cases} -1 \leq \beta \leq 1 \\ T_p = \frac{\Delta p V_p \beta}{2\pi} \eta_p \end{cases} \tag{1}$$

where β is the opening of the swashplate, $(-1, 1)$; Δp is the inlet and outlet pressure difference; V_p is the displacement; and η_p is the mechanical efficiency of the hydraulic pump/motor.

3.2. Electric Power

The battery is a very important power source in the MEH-DCDS. When the power is insufficient, the battery is used to provide part of the power, and at the same time, it can convert part of the braking energy into electrical energy for storage [30]. Therefore, the battery is the core of the hybrid drive system, and its dynamic characteristics analysis is very important. The total efficiency of the motor is 0.855, and the peak power of the battery pack should be greater than the maximum power of the motor; then, the formula for calculating the maximum power of the battery pack is as follows:

$$P_b = \frac{P\text{max}}{\eta \text{b}} \tag{2}$$

where P_{max} is the maximum power of the motor/generator design; P_b is the maximum power of the battery pack; and η_b is the total efficiency of the battery bank. Therefore, P_{max} = 30 kW is selected, and the maximum power of the battery pack P_b = 35 kW is calculated by substituting the parameters.

Choose a battery pack with a rated capacity of 65 Ah. The battery pack consists of a number of cells. The monoblocks are arranged in series. Initially, the rated voltage U_{bc} of the NiMH cell is 1.29 V. According to the maximum power of the battery pack design, the total number of cells n_{bc} of the battery pack is calculated as follows:

$$P\text{bc} = \frac{U\text{bc}^2}{4 \cdot R\text{bc}} \tag{3}$$

$$n\text{bc} = \frac{1000 \cdot P\text{max}}{P\text{maxc}} \tag{4}$$

where U_{bc} is the rated voltage of the single cell and R_{bc} is the internal resistance of the single cell. The mean value of 0.0026 Ω is taken here.

According to the calculated total number of cells, n_{bc} = 219, and every 40 cells are connected in series according to the actual situation and the arrangement of the cells. Here it is rounded to 6 groups, so n_{bc} = 240 is selected. The formula for calculating the rated voltage of the battery pack is:

$$U\text{b} = n\text{bc} \cdot U\text{bc} \tag{5}$$

The nominal voltage of the battery pack is calculated to be U_b = 310 V. Figure 2 shows the schematic diagram of the battery pack. The specific parameters of the battery pack are shown in the Table 1 below.

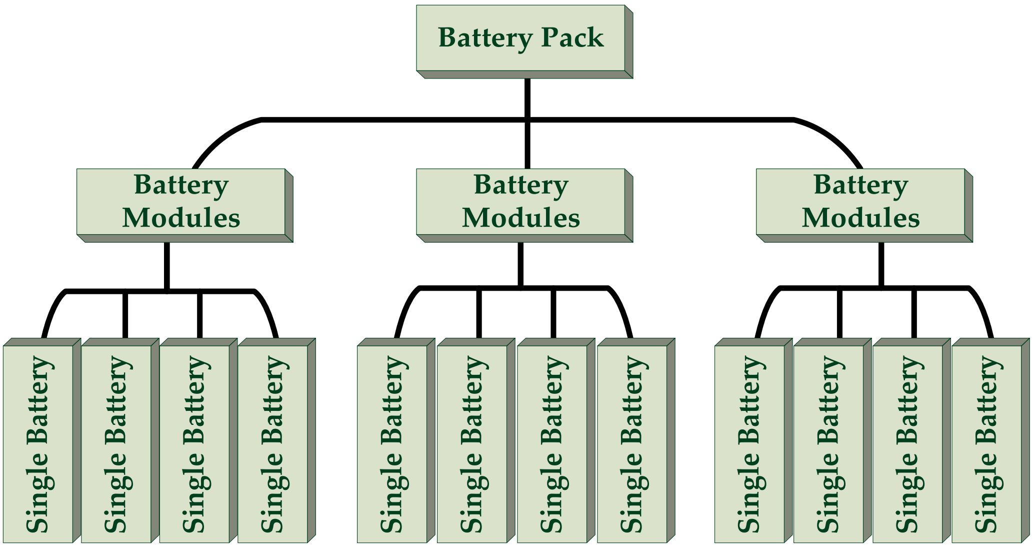

Figure 2. Schematic diagram of the battery pack.

Table 1. Battery pack parameters.

Battery Pack Parameters	Value	Unit
Voltage of the battery pack	310	V
Maximum power of the battery pack	35	kw
Battery pack capacity	65	Ah
Number of battery modules connected in parallel	1	None
Number of battery modules in series	6	None
Number of individual cells in series per module	40	None

In the MEH-DCDS, the motor is used to drive the vehicle to accelerate, charge when the energy of the accumulator is insufficient, and recover the braking energy during braking. The input torque of the motor T_{req} is subject to a limited torque limit of T_{lim}:

$$T_{\mathrm{min}} \le T_{\mathrm{lim}} \le T_{\mathrm{max}} \tag{6}$$

where T_{min} is the minimum torque of the motor, and T_{max} is the maximum torque of the motor.

The output torque T_{m} of the motor is determined from the limit torque T_{lim} using a first-order lag:

$$T_{\mathrm{m}} = \frac{1}{1 + t_{\mathrm{r}} \cdot s} \cdot T_{\mathrm{lim}} \tag{7}$$

where t_{r} is a user-defined time constant.

The mechanical power P_{mec} and power loss P_{lost} of the motor are calculated as follows:

$$\begin{cases} P\mathrm{mec} = \frac{T\mathrm{m} \cdot n\mathrm{e}}{9549} \\ P\mathrm{lost} = (1 - \eta\mathrm{e}) \cdot |P\mathrm{mec}| \end{cases} \tag{8}$$

where n_{e} is the rotary velocity of the motor shaft.

The different operating modes of the electric motor/generator can be illustrated in Figure 3.

So, the relation between the mechanical and the electric power is the following:

$$P\mathrm{elec} = P\mathrm{mec} - P\mathrm{lost} \tag{9}$$

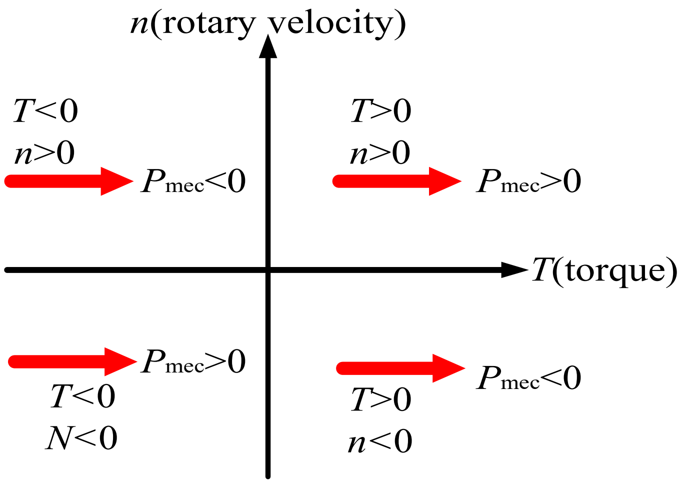

Figure 3. Diagram of the different modes of operation of the motor/generator.

The motor/generator efficiency corresponds to:

$$\begin{cases} \eta m = 2 - \frac{P_{elec}}{Pmec} \\ \eta g = \frac{Pelec}{Pmec} \end{cases} \tag{10}$$

where P_{elec} is the electric power; η_m is the motor efficiency; and η_g is the generator efficiency.

3.3. Hydraulic Accumulator

As the starting power source of the MEH-DCDS, the hydraulic accumulator is also the storage unit of braking energy recovery. Compared with batteries, it has the characteristics of fast starting and a large instantaneous torque. According to Boyle's law, the relationship between pressure and volume is

$$P_0 v_0{}^{\mathrm{n}} = P_1 v_1{}^{\mathrm{n}} = P_2 v_2{}^{\mathrm{n}} \tag{11}$$

where P_0 is the pre-charging pressure of the gas; v_0 is the accumulator charging volume; P_1 is the lowest working pressure of the accumulator; v_1 is the gas volume before the accumulator works; P_2 is the accumulator maximum working pressure; and v_2 is the gas volume after the accumulator works.

When the accumulator is working, there can be three modes, and its dynamic calculation depends on the accumulator mode:

(1) If the energy of the accumulator is sufficient, the gas pressure of the accumulator is at the maximum, and the volume is at the minimum, hence:

$$\begin{cases} P_{gas} = P_{max} \\ V_{gas} = \frac{V_0}{1000} \end{cases} \tag{12}$$

where P_{gas} is the gas pressure; P_{max} is the maximum pressure; V_{gas} is the gas volume; and V_0 is the accumulator volume.

(2) If the accumulator has been completely discharged, the gas pressure of the accumulator is at the pre-charge value, and the volume is at the maximum, hence:

$$\begin{cases} P_{gas} = P_0 \\ V_{gas} = V_0 \end{cases} \tag{13}$$

(3) If the accumulator is neither fully discharged nor fully charged, the air pressure is identical to the hydraulic pressure:

$$P_{gas} = P_{out} \tag{14}$$

where P_{out} is the output pressure of the accumulator.

The volume of gas is calculated using the law of many parties:

$$V_{gas} = V_0 \cdot \left(\frac{P_0}{P_{gas}} \right)^{\frac{1}{\gamma}} \tag{15}$$

4. Analysis of the Working Mode and Energy Management Strategies

The MEH-DCDS has multiple working modes. As shown in Figure 4, the working modes of the MEH-DCDS are roughly divided into five types [31,32]. Each working mode is independent of the other working modes. When formulating the control strategy according to different working conditions, this paper formulates the ruled control strategy of the MEH-DCDS. In the AMESim software, the formulation of the control strategy is realized through the construction of formulas. The vehicle speed threshold and the pressure of the high-pressure accumulator are used as the basis for mode switching to complete the simulation of the system. Figure 5 shows the control strategy of the MEH-DCDS.

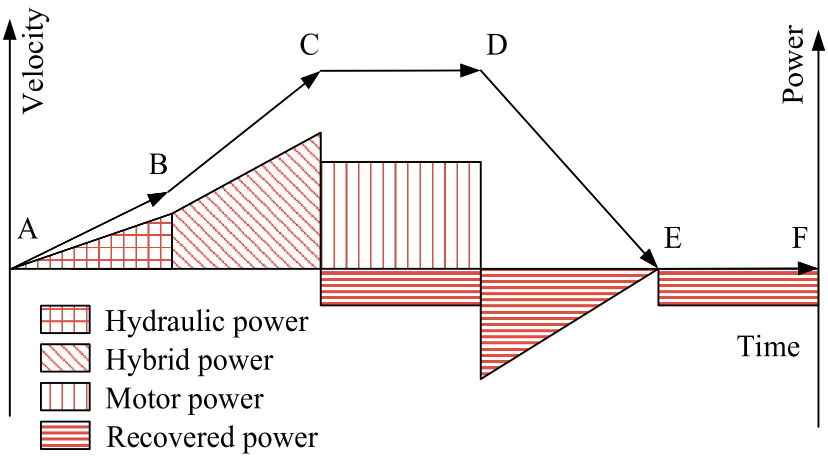

Figure 4. Working mode diagram of the MEH-DCDS.

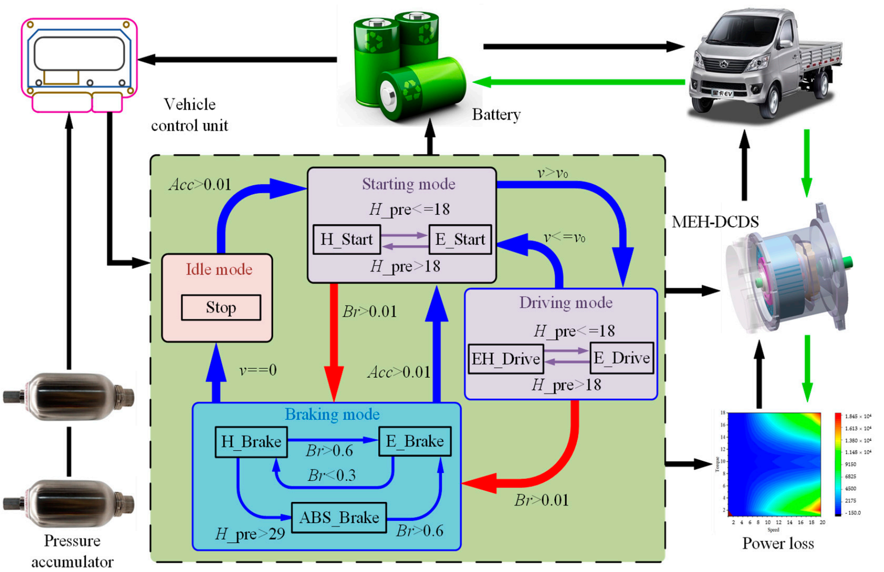

Figure 5. Energy management strategies of the MEH-DCDS.

(1) Starting mode: As shown in section AB, the starting torque of the vehicle is greater during starting. The required peak torque makes the battery pack in a high current discharge state, which has a greater effect on the battery SOC. Therefore, when the vehicle begins to accelerate, only the hydraulic system drives the vehicle. When the pressure of the high-pressure accumulator in the hydraulic system is greater than the pressure of the low-pressure accumulator, the secondary element works in the motor state. All the solenoid valve switches are turned on. At this time, the hydraulic oil in the high-pressure accumulator flows to the low-pressure accumulator. The oil drives the hydraulic motor to rotate and converts the hydraulic energy stored in the hydraulic accumulator into mechanical energy. When the pressure is lower than the minimum working pressure of the accumulator, the hydraulic accumulator cannot release the hydraulic oil. At this time, the battery pack drives the electric motor/generator to charge the hydraulic accumulator.
(2) Acceleration/climbing mode: As shown in section BC, the torque required for the vehicle to climb or accelerate must be sufficiently large to meet the driving requirements. After the vehicle is started, it accelerates to the vehicle speed threshold, and the battery pack begins to provide electrical energy. The electrical energy is converted into mechanical energy through the motor and coupled with hydraulic energy torque to achieve power mixing. It outputs electrical energy and hydraulic energy together as mechanical energy, which is converted into kinetic energy by the wheels to drive the vehicle to reduce the electrical power and current impact and increase the driving range.
(3) Constant speed mode: As shown in the CD section, under uniform speed conditions, the traction of the vehicle needs only to overcome frictional resistance and slope resistance. The external load of the vehicle is relatively small during the start and acceleration conditions. At this time, the solenoid valve switch is closed, the hydraulic system does not operate, and the electric power alone outputs torque to drive the vehicle at a constant speed. Under this working condition, the motor can work in a high-efficiency region to a large extent. In addition, when the output power of the motor is large, the abundant power of the motor can also charge the hydraulic accumulator to further improve its operating point, not only to make the motor work stably in the high-efficiency region but also to reserve for operating conditions that require instantaneous high-power energy.
(4) Braking mode: As shown in section DE, when the vehicle is decelerating and braking, the regenerative braking energy is converted into hydraulic energy and recycled into the high-pressure accumulator. The remaining energy is converted into electrical energy by the generator and stored in the battery, which reserves a certain amount of hydraulic energy for the vehicle's starting and acceleration conditions.
(5) Idle mode: As shown in section EF, when the vehicle is idling, the electric power does not output mechanical energy to the outside. Instead, it converts electrical energy into hydraulic energy to charge hydraulic accumulators, which store energy for vehicle starting and working conditions that require instantaneous high power.

In summary, the MEH-DCDS control strategy is primarily designed for how to select the power source under different operating conditions of the vehicle. For the study of the MEH-DCDS, the expected vehicle speed is used as the control input signal, and the battery SOC and the pressure and energy storage conditions of the high- and low-pressure accumulators are monitored in real-time to achieve the desired effect of the actual vehicle speed. Table 2 shows the energy flow direction of different working modes.

Table 2. Working modes of the MEH-DCDS.

Working Mode	Power Source		Diagram of Energy Flow
	Motor	Hydraulic Pump/Motor	
Starting mode	—	Hydraulic motor	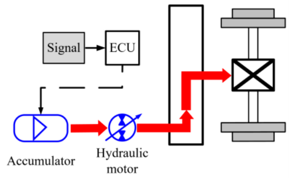
Acceleration/climbing mode	Motor	Hydraulic motor	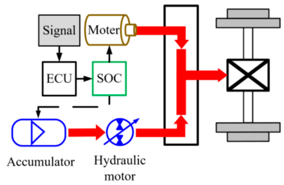
Constant speed mode	Motor	—	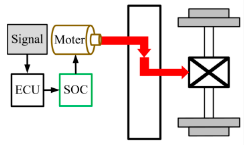
Braking mode	Generator	Hydraulic pump	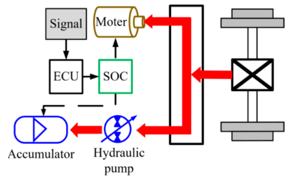
Idle mode	Motor	Hydraulic pump	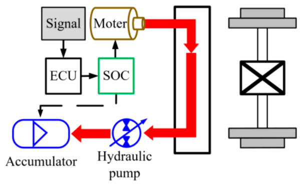

5. Simulation and Analysis

5.1. Basic Parameters

The parameters of the MEH-DCDS are based on the dynamic requirements of the vehicle. The fundamental parameters are shown in Table 3.

Table 3. Basic parameters of the MEH-DCDS.

Components	Parameters	Value
Basic parameters of the vehicle	Loaded mass (m)	1206 kg
	Frontal area (A)	2.28 m^2
	Rolling resistance coefficient (f)	0.0135
	Coefficient of air resistance (C_D)	0.32
	Wheel width (R)	290 mm
	Transmission efficiency (η)	0.85
High pressure accumulator	Work pressure (P_1)	24–35 MPa
	Volume (V)	35 L
Low pressure accumulator	Work pressure (P_2)	6–22 MPa
	Volume (V)	35 L
Secondary component	Displacement (V_p)	30 mL·r^{-1}
Motor	Rated power (P_e)	32 kW

5.2. Simulation Model

The MEH-DCDS simulation model established in the AMESim software is shown in Figure 6. The vehicle powertrain model consists of a motor model, a battery model, a wheel model, and a road model. The mass block is used to simulate the mass of the entire vehicle and the load resistance. The torque after the electric motor and the hydraulic motor are coupled is transformed into the driving force input of the mass block.

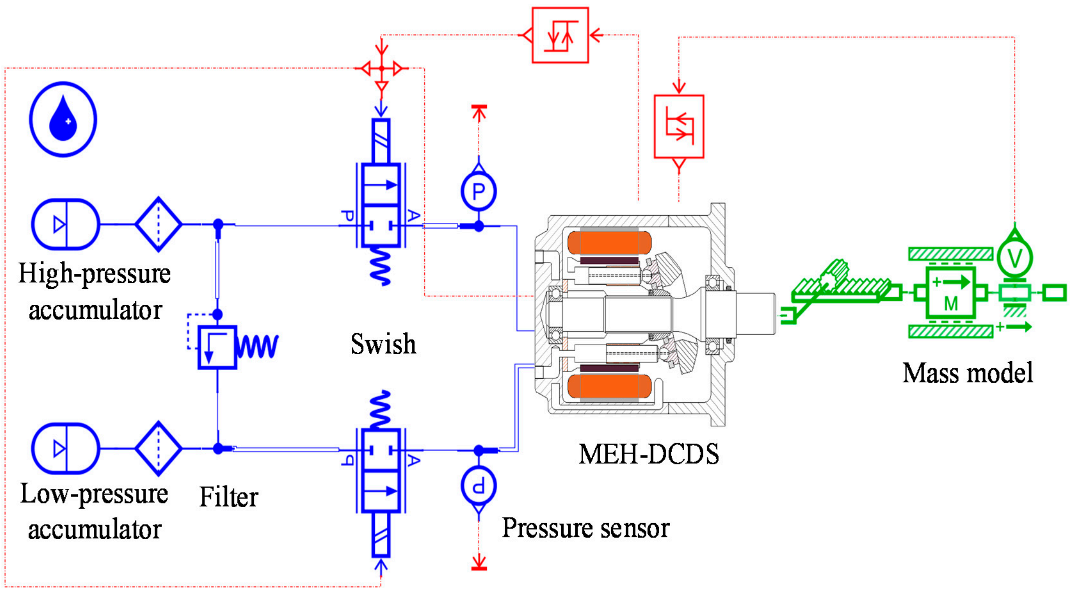

Figure 6. MEH-DCDS model constructed using the AMESim software.

The MEH-DCDS integrates the secondary component and the motor. It is represented as a whole in Figure 6, and in AMESim it is composed of a motor model, hydraulic pump/motor model, hydraulic signal, switch, coupling mechanism, etc., as shown in Figure 7.

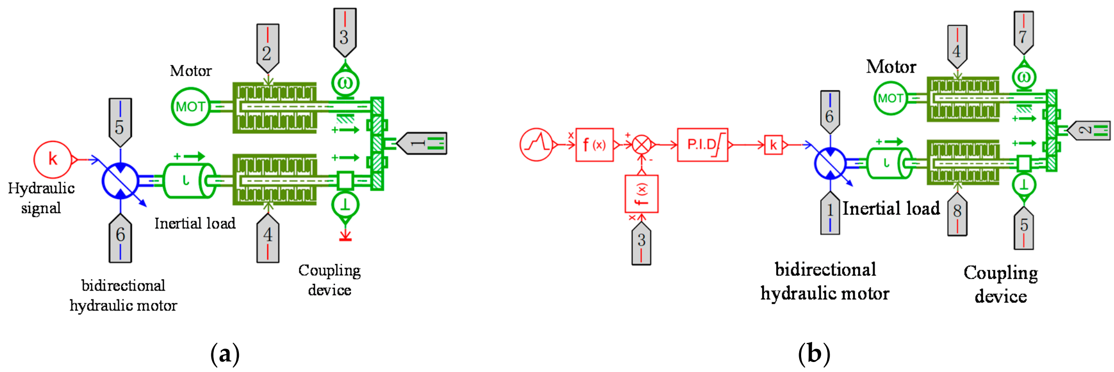

Figure 7. Internal structure of the MEH-DCDS: (**a**) is the MEH-DCDS model, and (**b**) is the MEH-DCDS model under PID control.

5.3. Analysis of the Simulation Results

(1) Analysis of the starting characteristics

It is assumed that the vehicle is started by hydraulic power, and after reaching the vehicle speed threshold of 5/3.6 m/s, the electric power works together. After reaching a constant speed, the hydraulic system is closed, and only electric power drives the vehicle to travel at a constant speed. The switch signal of the first two sections is 40, which means the switch is open. The switch signal of the latter period is 0, indicating that the switch is closed (see Figure 8).

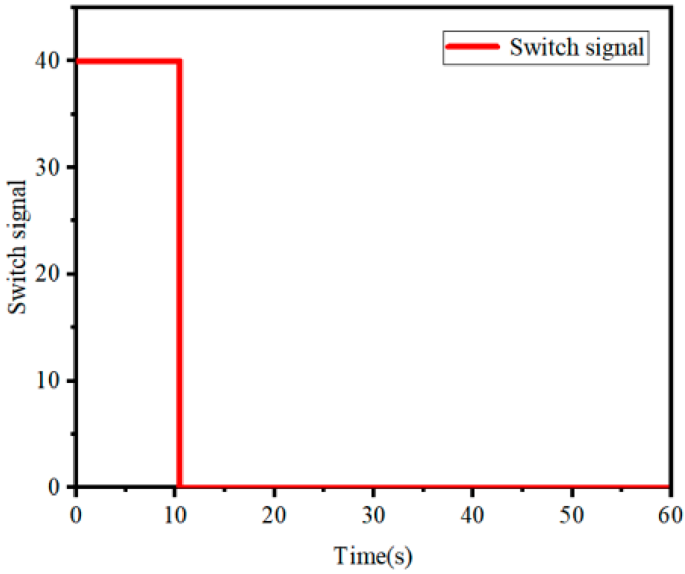

Figure 8. Diagram of the switch signal.

The starting characteristics of the MEH-DCDS and purely motor drive systems were analyzed. In AMESim, the swashplate signal input is 1, and the swashplate remains fully open. At this time, the secondary element is used as a hydraulic motor. In a purely motor system, a swashplate signal input of 0 means it is closed. The hydraulic system does not work, and there is only electric power drive. Curve 1 represents the vehicle speed curve of the MEH-DCDS, and Curve 2 represents the vehicle speed curve of a purely electric system vehicle. Figure 9 shows that the starting time of the purely motor system is 7.58 s, and the acceleration to constant speed is 14.62 s. However, the MEH-DCDS has a starting time of 4.52 s and an acceleration to a constant speed of 10.43 s. The starting performance is improved by 40.37%, and the acceleration performance is improved by 16.05%. In terms of power, the MEH-DCDS has a faster start and acceleration response, and the acceleration time is shorter than that of a purely motor-driven vehicle.

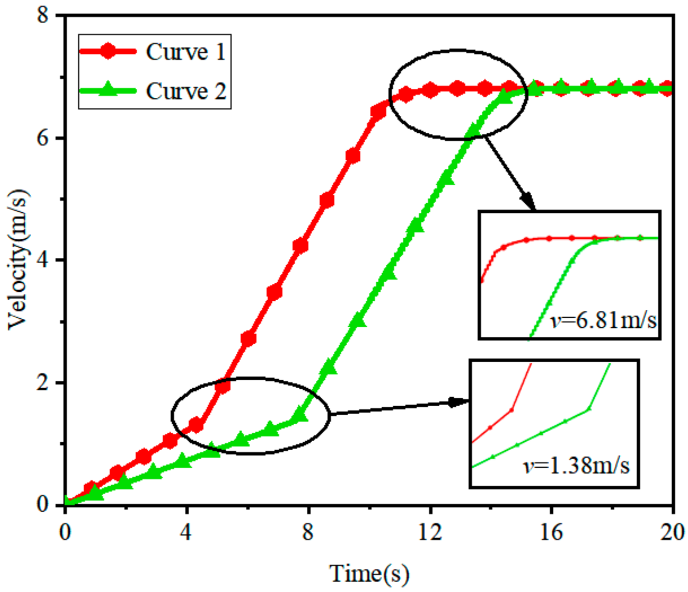

Figure 9. Diagram of the vehicle speed comparison.

(2) Torque analysis during driving

Figure 10 shows the various torques and their distribution for the MEH-DCDS during driving. As shown in the figure, the torque of the hydraulic motor quickly reaches its peak value. When the vehicle has barely started, the electric power does not operate, and the electric power output torque is 0. When the vehicle begins to reach the speed threshold, it enters the acceleration phase. At this time, the electric power is involved in the work, and the output torque of the electric power increases instantly. The output torque of the MEH-DCDS begins to decrease as the motor speed and power stabilize. The electric power and hydraulic power output work together, and the torque of the hydraulic motor also shows a slight downward trend. When entering the uniform speed phase, the external load of the vehicle is relatively small when starting and accelerating. The MEH-DCDS closes the switch and the torque of the hydraulic motor drops to 0. At this time, the hydraulic system will no longer operate. When the motor enters the uniform speed stage, the output torque of the motor tends to be flat as the inertia effect decreases, and the final output torque remains constant so that the electric power works in the high-efficiency region.

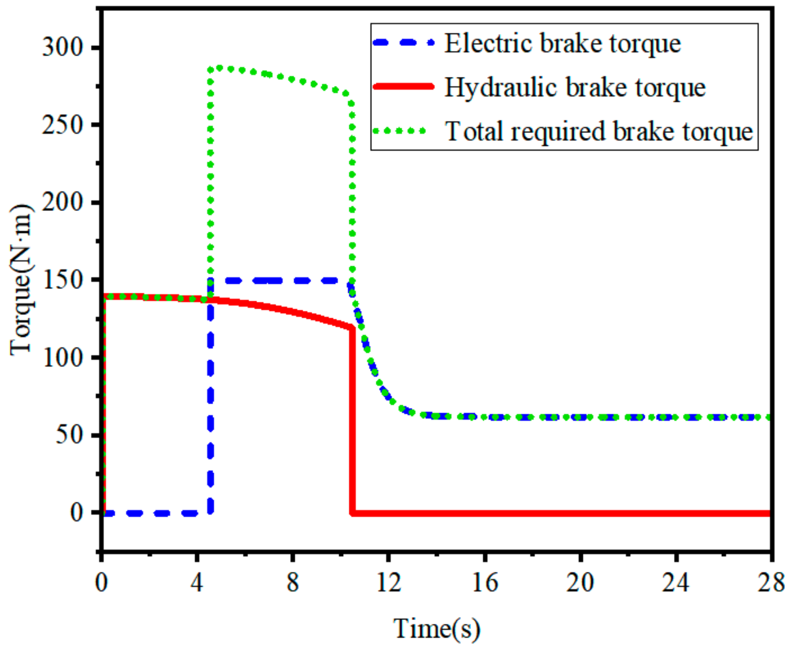

Figure 10. Diagram of the output torque.

(3) Analysis of the discharge characteristics of the accumulator

Figure 11 shows the change curve of the oil pressure and gas volume for the high- and low-pressure accumulators. The figure shows that the gas volume and oil pressure changes of the high- and low-pressure accumulators undergo opposite trends. When the hydraulic system is working, the oil pressure of the high-pressure accumulator decreases, and the oil pressure of the low-pressure accumulator increases. Because the oil produces a vortex, impact, friction, etc., when it flows through the pipeline, it consumes a part of the energy and causes the increasing pressure to be lower than the released pressure. The gas volume of the low-pressure accumulator decreases as the pressure increases, and the gas volume of the high-pressure accumulator increases as the pressure decreases. The figure shows that a small reduction in the pressure of the accumulator is sufficient to provide the vehicle with instantaneous starting torque, and much hydraulic oil remains stored in the high-pressure accumulator, which is sufficient for the acceleration or even a second start of the vehicle.

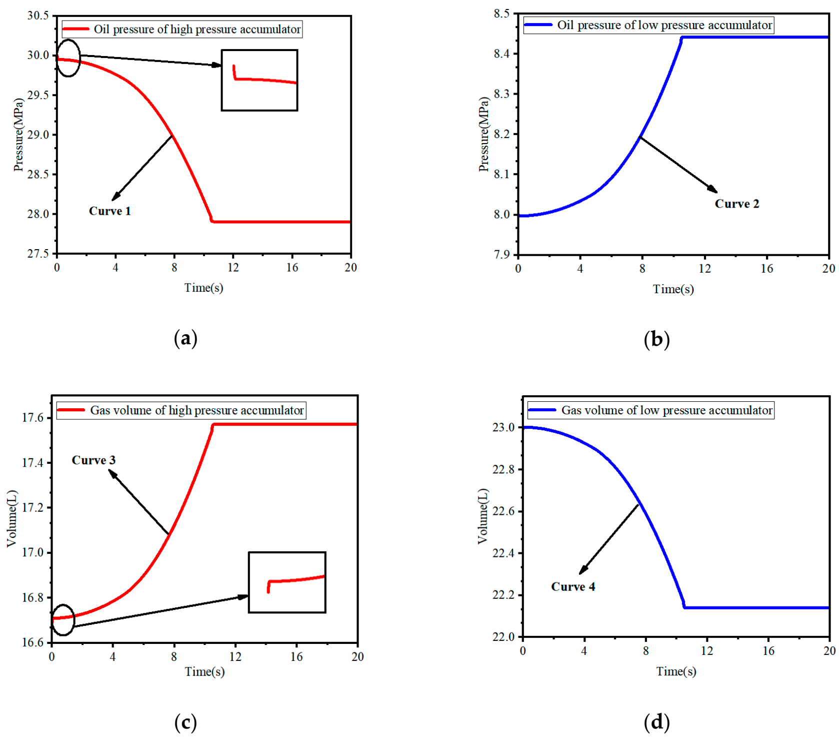

Figure 11. Diagrams of the pressure and gas changes of the accumulator. (**a**) is the curve of oil pressure in high pressure accumulator, (**b**) is the curve of oil pressure in low pressure accumulator, (**c**) is the curve of gas volume in high pressure accumulator, and (**d**) is the curve of gas volume in low pressure accumulator.

(4) Research on PID regulation control

Curve 3 represents the speed of the MEH-DCDS vehicle after PID control. Curve 2 represents the speed of a purely electric vehicle. The time for the MEH-DCDS vehicle to reach the speed threshold is 4.52 s. To make the vehicle start faster, PID control is adopted for the hydraulic pump/motor. Figure 12 shows that under the PID regulation control, the MEH-DCDS vehicle reaches the starting speed threshold in 3.48 s, and the acceleration performance is improved by 23.01%. Compared with the acceleration performance of the purely electric vehicle, that of the MEH-DCDS vehicle is greatly improved, and the power performance is well improved.

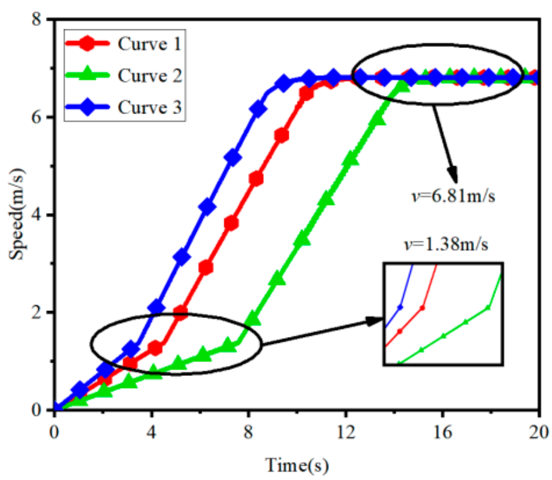

Figure 12. Diagram of the vehicle speed under different controls.

Figure 13 shows the change curve of the oil pressure and gas volume of the MEH-DCDS with and without PID control. After PID adjustment, the oil pressure of the high-pressure accumulator is reduced by 0.236 MPa and the gas volume is reduced by 0.09683 L. Therefore, the accumulator can further improve the acceleration performance of the vehicle under the condition of releasing less oil, greatly improving the dynamic performance of the vehicle, and can greatly increase the driving range of the vehicle.

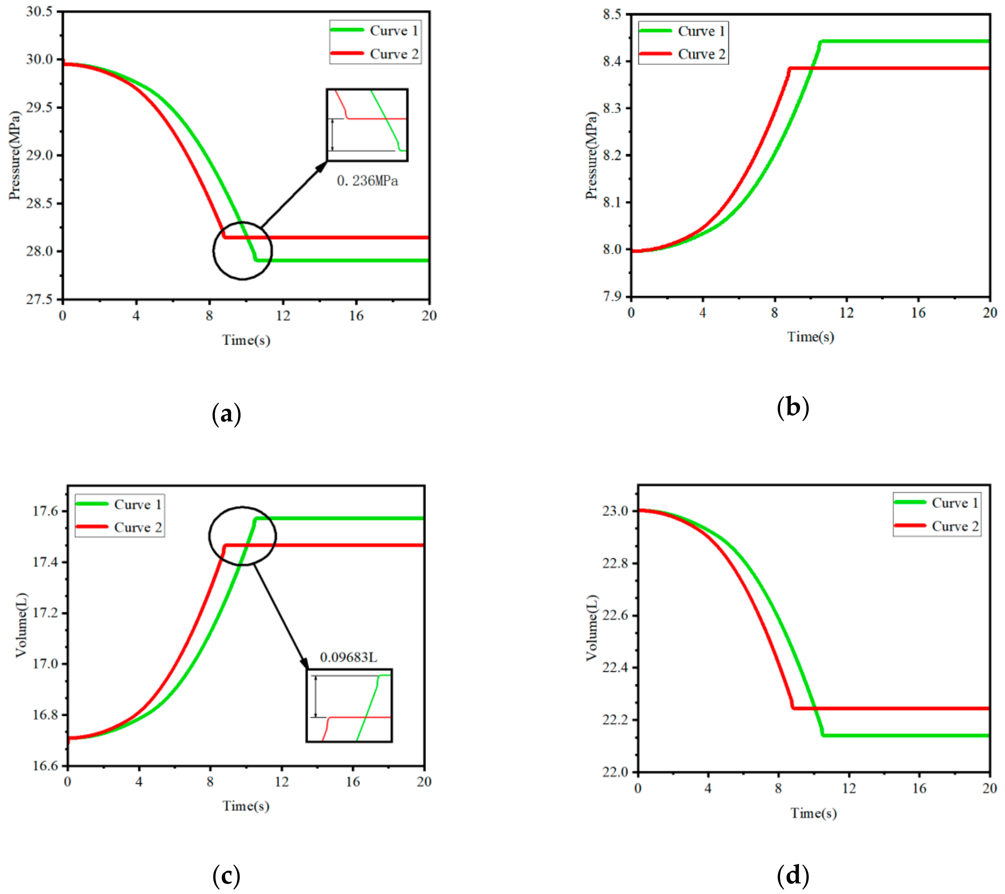

Figure 13. Diagrams of the oil pressure and gas volume of the MEH-DCDS with and without PID control. (**a**) is the comparison chart of oil pressure in high pressure accumulator, (**b**) is the comparison chart of oil pressure in low pressure accumulator, (**c**) is the comparison chart of gas volume in high pressure accumulator, and (**d**) is the comparison chart of gas volume in low pressure accumulator.

6. Verification Based on Cyclic Conditions

6.1. Whole Vehicle Modeling

The dynamics of the MEH-DCDS has been verified previously. The results of the validation are sufficient to demonstrate the feasibility of the system. The system is now integrated into the complete vehicle. A joint simulation using AMESim/Simulink is used to verify the feasibility of the MEH-DCDS based on the certification cycle.

In recent years, NEDC (new European driving cycle, NEDC) has become the most widely used driving cycle in the world. Therefore, this paper adopts NEDC to verify the driving conditions of the MEH-DCDS. The modeling and simulation diagram of the whole vehicle is shown in Figure 14. As can be seen in the figure, the MEH-DCDS has internal interface #2 for the electrodynamic signal and interface #1 for the hydraulic power signal. The co-simulation interface is connected to the Simulink module. The control flow is shown in Figure 3.

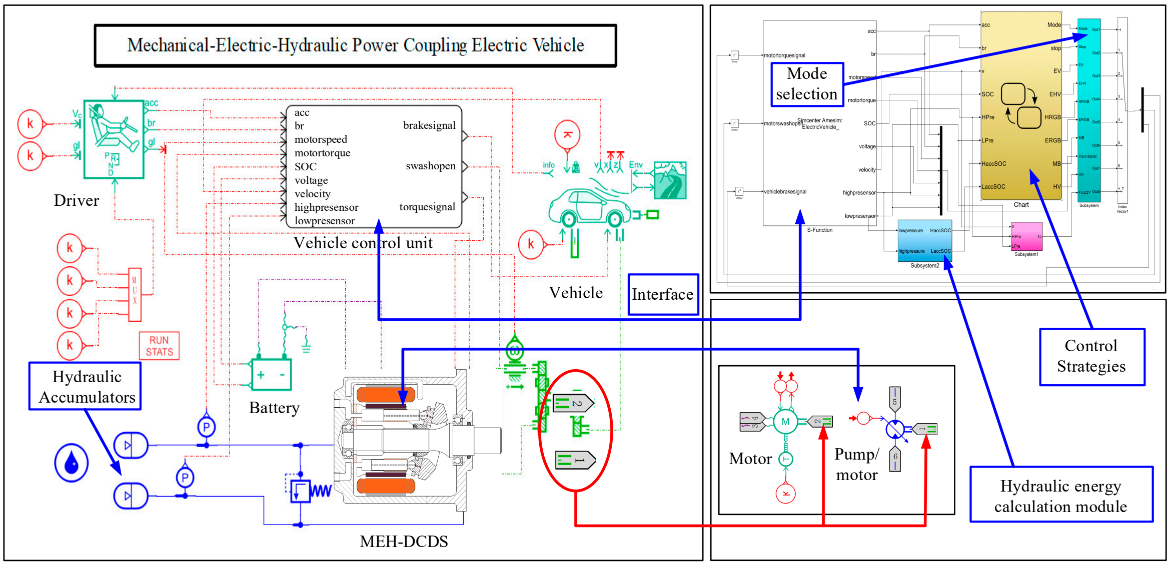

Figure 14. Model drawing of the whole car.

6.2. Results and Analysis of Validation

Figure 15 shows the speed and pressure curves. Figure 16 shows the swashplate signal curve. After the joint verification of AMESim/Simulink, the speed curve of the MEH-DCDS can follow the control vehicle speed well, as shown in the figure. The curves basically overlap, and there is no serious out-of-curve problem. At the same time, the pressure of the high- and low-pressure accumulators can be changed continuously with a change in vehicle speed. The swashplate signal is positive when the vehicle speed is rising. At this time, the HPA pressure goes down and the LPA pressure goes up. When the speed is decreasing, the swashplate signal is negative. The HPA pressure goes up and the LPA pressure goes down. This is basically in line with the original design concept.

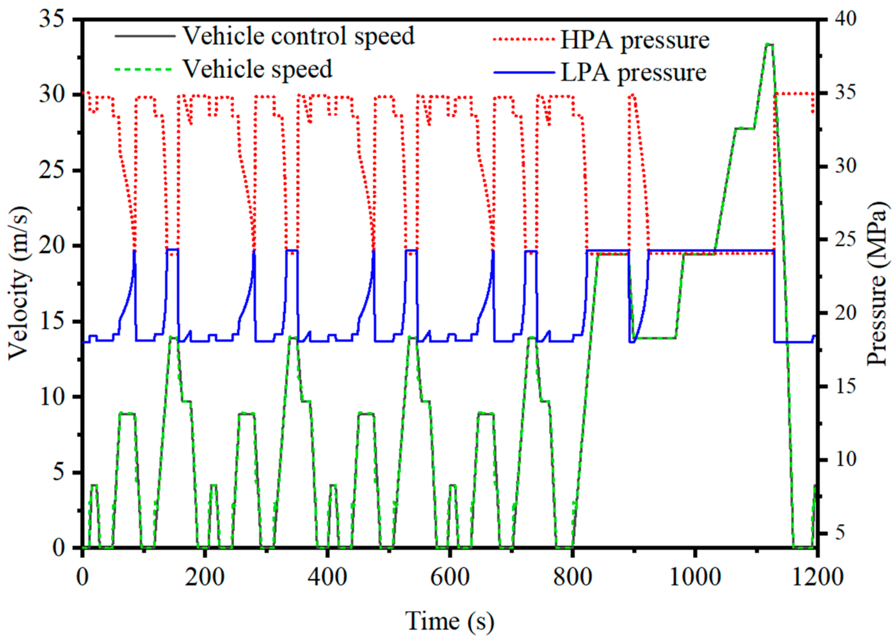

Figure 15. Diagram of the speed and pressure curves.

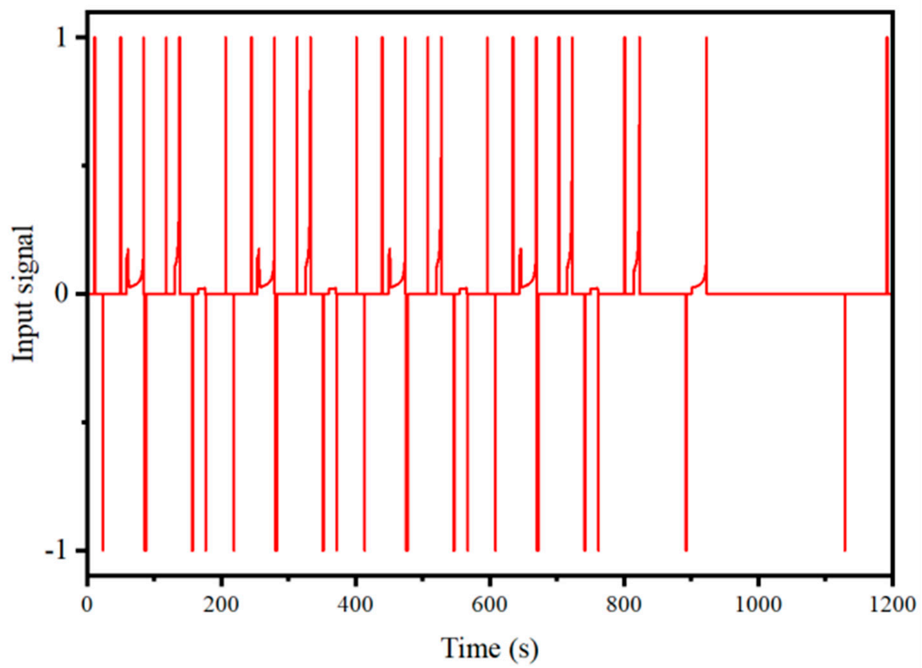

Figure 16. Diagram of the swashplate signal curve.

Figure 17 shows the curves of the battery SOC consumption rate for the MEH-DCDS and EV. It can be seen from the graph that the battery SOC remaining for the MEH-DCDS is 94.7363% and the battery SOC remaining for the EV is 93.3931%, with a 20.33% reduction in the energy consumption rate. Figure 18 shows the mileage comparison between the MEH-DCDS and the EV under the NEDC cycle condition. It can be seen that the vehicle has a mileage of 11.0041 km when driven by hydraulic power, while the EV has a mileage of 10.9584 km, an increase of 45.7 m compared to the EV.

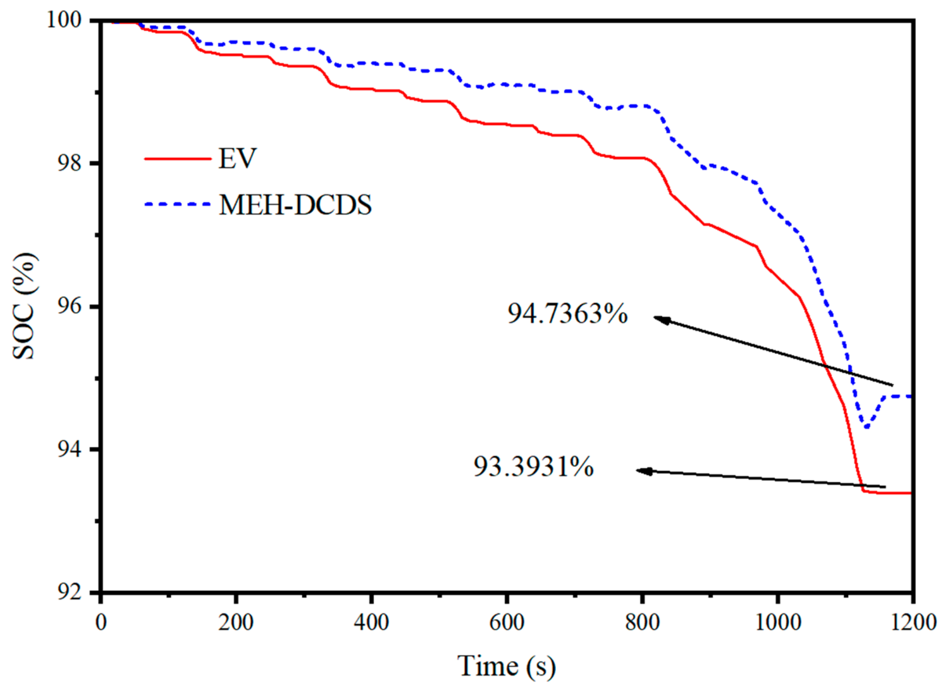

Figure 17. Comparison of the state-of-charge (SOC) consumption rates.

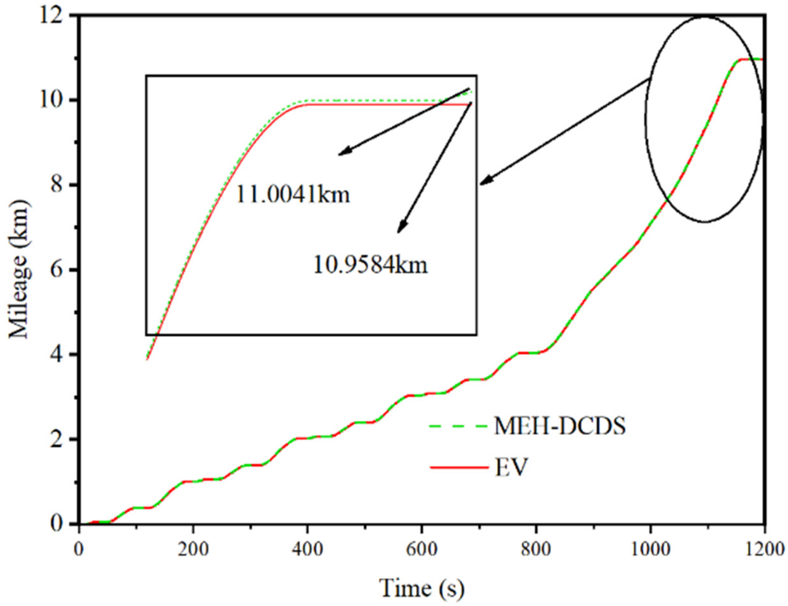

Figure 18. Comparison of mileage.

7. Conclusions

A new type of electro-hydraulic power coupler (MEH-DCDS) is proposed. It integrates the traditional permanent magnet rotating motor with the swashplate axial piston pump/motor, which can realize the mutual conversion of electrical energy, mechanical energy, and hydraulic energy. This article explains its working principle and advantages. At the same time, its key components are modeled to complete the structural realization of the vehicle model. According to the MEH-DCDS design principle, the different modes of operation of a vehicle are classified. The energy flow in different driving modes is not the same, so the driving energy of the vehicle under different operating conditions is studied. Based on this principle, an energy management strategy based on different operating conditions is designed. The results of the validation can demonstrate the feasibility of the system.

Based on the AMESim software platform, the starting acceleration performance of the MEH-DCDS and purely electric drive system is simulated and analyzed. The results show that the start time of the purely electric drive system is 7.58 s, while that of the MEH-DCDS is 4.52 s, and the starting performance is improved by 40.37%.

Based on the dynamic model of the MEH-DCDS, a control method combining real-time feedback of hydraulic power output torque and PID control is proposed. The output torque is calculated by a formula and fed back to the input signal. After the PID adjustment, the oil drainage of the MEH-DCDS is greatly reduced, and the starting time of the vehicle is shortened by 1.04 s, while the starting time is shortened by 1.04 s and the acceleration performance is improved by 23.01%, which greatly improves the power performance of MEH-DCDS.

The dynamic performance of the MEH-DCDS was verified by the AMESim model. The system is now integrated into the whole vehicle. The dynamic performance of the MEH-DCDS under cycle conditions was verified by using AMESim to build a model of the whole vehicle, Simulink software to build a control strategy, and co-simulation methods to verify the dynamic performance of the MEH-DCDS under cycle conditions. The vehicle runs for one NEDC certification cycle after loading the MEH-DCDS, and the MEH-DCDS is able to follow the control vehicle speed well. The SOC consumption rate was reduced by 20.33% compared to a purely electric vehicle, and the MEH-DCDS has an increased range of 45.7 m compared to the EV. Finally, the proposed new structure is proven to be feasible in terms of dynamics and vehicle application.

Ultimately, the new structure proposed in this paper can not only improve the vehicle's dynamic performance, but also improve its energy efficiency. After applying the system to the vehicle, it is verified that the simulation can significantly reduce the SOC consumption and increase the mileage of the vehicle. This will provide a good basis for further research ideas pertaining to the study of electro-hydraulic hybrid power systems.

Author Contributions: Conceptualization, Z.M.; Data curation, J.Y.; Formal analysis, J.Y. and J.H.; Methodology, T.Z., H.Z., J.H. and Z.M.; Resources, J.Y., T.Z., H.Z. and J.H.; Writing – original draft, J.Y.; Writing—review & editing, J.Y. and J.H. All authors have read and agreed to the published version of the manuscript.

Funding: This research was funded by the National Natural Science Foundation of China, grant number 52075278, and Municipal Livelihood Science and Technology Project of Qingdao, grant number 19-6-1-92-nsh.

Conflicts of Interest: The authors declare no conflict of interest.

References

1. Hong, J.C.; Wang, Z.P.; Zhang, T.Z. Research on Performance Simulation of Load Isolation Pure Electric Driving Vehicles. *Energy Procedia* **2016**, *104*, 544–549. [CrossRef]
2. Zhang, N.; Chen, X.; Yu, M. Materials chemistry for rechargeable zinc-ion batteries. *Chen. Soc. Rev.* **2020**, *49*, 4203–4219. [CrossRef] [PubMed]
3. Lu, L.; Han, X.; Li, J.; Hua, J.; Ouyang, M. A review on the key issues for lithium-ion battery management in Electric Vehicles. *J. Power Sources* **2013**, *226*, 272–288. [CrossRef]
4. Liu, K.; Luo, S.; Zhou, J. En-Route Battery Management and a Mixed Network Equilibrium Problem Based on Electric Vehicle Drivers' En-Route Recharging Behaviors. *Energies* **2020**, *13*, 16. [CrossRef]
5. Wu, Y.; Jiang, X.H.; Xie, J.Y. The reasons of rapid decline in cycle life of Li-ion battery. *Battery Bimon.* **2009**, *39*, 206–207.
6. Deng, L.Z.; Wu, F.; Gao, X.G.; Wu, W. Development of a LiFePO4-based high power lithium secondary battery for HEVs applications. *Rare Met.* **2014**, *39*, 1457–1463. [CrossRef]
7. Guo, W.; Cong, Z.; Guo, Z.; Chang, C.Y.; Pu, X. Dendrite-free Zn anode with dual channel 3D porous frameworks for rechargeable Zn batteries. *Energy Storage Mater.* **2020**, *30*, 104–112. [CrossRef]
8. Wang, L.; Wang, X.; Yang, W. Optimal design of electric vehicle battery recycling network—From the perspective of electric vehicle manufacturers. *Appl. Energy* **2020**, *275*, 115328. [CrossRef]
9. Zhao, K.G.; Liang, Z.H.; Huang, Y.J.; Wang, H.; Khajepour, A.; Zhen, Y.K. Research on a Novel Hydraulic/Electric Synergy Bus. *Energies* **2017**, *11*, 34. [CrossRef]
10. Fiala, S.; Bubak, A.; Novotny, L. Control of hybrid electric-hydraulic drive for vertical feed axes of machine tools. *MM Sci. J.* **2019**, *2019*, 3228–3235. [CrossRef]
11. Sun, H.; Jing, J.Q. Research on the System Configuration and Energy Control Strategy for Parallel Hydraulic Hybrid Loader. *Automat. Constr.* **2010**, *19*, 213–220.
12. Pugi, L.; Pagliai, M.; Nocentini, A.; Lutzemberger, G.; Pretto, A. Design of a hydraulic servo-actuation fed by a regenerative braking system. *Appl. Energy* **2017**, *187*, 96–115. [CrossRef]
13. Wang, J. Hierarchical Model Predictive Control for Hydraulic Hybrid Powertrain of a Construction Vehicle. *Appl. Sci.* **2020**, *10*, 745. [CrossRef]
14. Pretto, A.; Pugi, L.; Pugi, L.; Giglioli, M.; Berzi, L.; Locorotondo, E. Simulation and design of a kit for the electrification of a light tricycle truck. *Int. J. Heavy Veh. Syst.* **2020**, *27*, 278–302. [CrossRef]
15. Zhou, S.; Walker, P.; Tian, Y.; Zhang, N. Mode switching analysis and control for a parallel hydraulic hybrid vehicle. *Veh. Syst. Dyn.* **2020**. [CrossRef]
16. Niu, G.; Shang, F.; Krishnamurthy, M.; Garcia, J.M. Design and Analysis of an Electric Hydraulic Hybrid Powertrain in Electric Vehicles. *IEEE Transp. Electr.* **2016**, *3*, 48–57. [CrossRef]
17. Hwang, H.Y.; Lan, T.S.; Chen, J.S. Optimization and Application for Hydraulic Electric Hybrid Vehicle. *Energies* **2020**, *13*, 322. [CrossRef]
18. Sprengel, M.; Ivantysynova, M. Recent Developments in a Novel Blended Hydraulic Hybrid Transmission. *SAE Tech. Pap.* **2014**, *2014*. [CrossRef]
19. Niu, G.; Shang, F.; Krishnamurthy, M. Evaluation and selection of accumulator size in electric-hydraulic hybrid (EH2) powertrain. *ITEC* **2016**. [CrossRef]
20. Midgley, W.; Cathcart, C.D. Modelling of hydraulic regenerative braking systems for heavy vehicles. *Proc. Inst. Mech. Eng.* **2013**, *227*, 1072–1084. [CrossRef]

21. Wang, H.; Wang, Q. Parameter Matching and Control of Series Hybrid Hydraulic Excavator based on Electro-hydraulic. Composite Energy Storage. *IEEE Access* **2020**, *8*, 111899–111912. [CrossRef]
22. Zhou, H.C.; Xu, Z.P.; Liu, L.; Liu, D.; Zhang, L.L. Design and validation of a novel hydraulic hybrid vehicle with wheel motors. *Sci. Prog.* **2019**, *103*, 003685041987802. [CrossRef] [PubMed]
23. Nadeau, J.; Micheau, P.; Boisvert, M. Collaborative control of a dual electro-hydraulic regenerative brake system for a rear-wheel-drive electric vehicle. *Proc. Inst. Mech. Eng.* **2018**, *233*, 1035–1046. [CrossRef]
24. Zhao, W.Z.; Zhou, X.C.; Wang, C.Y.; Luan, Z.K. Energy analysis and optimization design of vehicle electro-hydraulic compound steering system. *Appl. Energy* **2019**, *255*, 113713. [CrossRef]
25. Liu, H.L.; Chen, G.P.; Xie, C.X.; Li, D.F.; Wang, J.W.; Li, S. Research on energy-saving characteristics of battery-powered electric-hydrostatic hydraulic hybrid rail vehicles. *Energy* **2020**, *205*, 118079. [CrossRef]
26. Li, J.S.; Zhao, J.Y.; Zhang, X.C. A Novel Energy Recovery System Integrating Flywheel and Flow Regeneration for a Hydraulic Excavator Boom System. *Energies* **2020**, *13*, 315. [CrossRef]
27. Hong, J.C.; Wang, Z.P.; Zhang, T.Z.; Yin, H.X.; Zhang, H.X.; Huo, W.; Zhang, Y.; Li, Y. Research on integration simulation and balance control of a novel load isolated pure electric driving system. *Energy* **2019**, *189*, 116220. [CrossRef]
28. Wu, W.; Di, C.; Hu, J. Dynamics of a hydraulic-transformer-controlled hydraulic motor system for automobiles. *Proc. Inst. Mech. Eng.* **2016**, *230*, 229–239. [CrossRef]
29. Golman, R.; Bhatia, S.; Kane, P.B. The dual accumulator model of strategic deliberation and decision making. *Psychol. Rev.* **2020**, *127*, 477–504. [CrossRef]
30. Xin, Y.F.; Zhang, T.Z.; Zhang, H.X.; Zhao, Q.H.; Zheng, J.; Wang, C.C. Fuzzy Logic Optimization of Composite Brake Control Strategy for Load-Isolated Electric Bus. *Math. Probl. Eng.* **2019**, *2019*, 9735368. [CrossRef]
31. Yang, Y.; Zhong, Z.; Wang, F.; Fu, C.Y.; Liao, J.Z. Real-time Energy Management Strategy for Oil-Electric-Liquid Hybrid System Based on Lowest Instantaneous Energy Consumption Cost. *Energies* **2020**, *13*, 4. [CrossRef]
32. Zhou, S.; Walker, P.; Zhang, N. Parametric design and regenerative braking control of a parallel hydraulic hybrid vehicle. *Mech. Mach. Theory* **2020**, *146*, 103714. [CrossRef]